Near threshold fatigue crack growth behavior of a third generation aluminium-lithium alloy

S. Richard*, C. Sarrazin-Baudoux, J. Petit
LMPM ENSMA, Futuroscope Chasseneuil, France

ABSTRACT

New generation aluminum-lithium alloys are good candidates in substituting to conventional aluminum alloys used in aeronautics. This paper deals with a contribution to the study of a 2050 T851 alloy damage tolerant properties. This alloy, showing an attractive combination of properties required for structural applications presents a resistance against crack propagation comparable to conventional alloys.

1 INTRODUCTION

Due to their good specific mechanical properties, aluminium alloys are widely used in aeronautics. The dramatic increase in fuel prices and the environmental considerations lead the aircraft designers to get interested in new lighter materials. In this context, the third generation aluminium lithium alloys are good candidates in substituting to conventional aluminium alloys, but their damage tolerant properties have to be studied before application. The resistance against crack propagation of three third generation aluminium-lithium alloys was compared in the Paris regime in a previous study [1], and in order to go further into the analysis, the near-threshold crack propagation behaviour of one of these alloys was investigated.

2 MATERIALS AND MICROSTRUCTURE

The 2050 third generation aluminium lithium alloy used in this study is provided by Alcan CRV in form of plate (15.5mm thick), at T851 temper. The 6mm thick CT specimens were machined in the core of the plate.
For comparison purpose, results coming from previous studies on a second generation 8090 7651 Al-Li alloy [2, 3] and conventional 2022 T851 Al-Cu-Mg alloy [4] are considered. Chemical compositions of the three alloys are given in Table 1.

* Corresponding author. E-mail : sebastien.richard@lmpm.ensma.fr

	Chemical composition (%wt)	Cu	Li	Mg	Mn	Ag	Si	Fe	Zn	Zr	Cr	Ti
2022	*min*	4.5	-	0.1	0.15	-			0.05	-		
	max	5.5		0.45	0.5		0.15	0.2	0.3		0.05	0.15
8090	*min*	1.1	2.2	0.7		-				0.08		
	max	1.7	2.8	1.3	0.1		0.2	0.3	0.25	0.16	0.1	0.1
2050	*min*	3.2	0.7	0.2	0.2	0.2				0.06	-	-
	max	3.9	1.3	0.6	0.5	0.7	0.08	0.1	0.25	0.14		

Table 1: Chemical composition of the 8090, 2022 and 2050 alloys.

The characteristics of the microstructure in terms of grain structure, grain size, and strengthening precipitate types are summarized in Table 2, and the main mechanical properties (E, $R_{p0.2}$, R_m, $A\%$ and K_{IC}) and density d are given in Table 3.

	Grain structure	Grain size (L*T*TC) *(µm)*	Strengthening precipitates
2022 T851	recrystallized	670*200*80	θ' (Al_2Cu)
8090 T651	partially recrystallized	30*15*10	δ'(Al_3Li) + S'(Al_2CuMg)
2050 T851	partially recrystallized	>1000*100*30	T_1(Al_2CuLi)

Table 2 : Microstucture of the studied alloys.

	Direction	E *(GPa)*	$R_{p0.2}$ *(MPa)*	R_m *(MPa)*	A%	K_{IC} *(MPa.m$^{1/2}$)*	d
2022 T851	L-T	72	380	440	14	41	2.80
8090 T651	T-L	81	420	510	7	29	2.54
2050 T851	T-L	77	500	530	11	37	2.70

Table 3 : Main mechanical properties and density of the studied alloys.

3 EXPERIMENTAL PROCEDURE

Crack propagation tests were performed on a servo hydraulic testing machine with a sinusoidal loading at a frequency of 35 Hz in ambient air, and 30 Hz in vacuum, on Compact Tension specimens with a width W of 50 mm and a thickness B of 6 mm, machined with a crack plane having a TL orientation. Threshold tests were performed at a load ratio R = 0.1 using a load-shedding procedure in accordance with ASTM recommendation. Crack advance was monitored by mean of a traveling microscope (accuracy of 0.01mm) in air or measured by mean of the potential drop technique when tests were carried out in vacuum. Closure correction was made using the compliance-offset method [5, 6] by means of back-face strain gauges, or using a capacitive sensor mounted at the mouth of the notch for tests run in vacuum.

4 NEAR THRESHOLD FATIGUE CRACK PROPAGATION

Growth rate da/dN is plotted with respect to the stress intensity factor range ΔK in a log-log diagram as shown in Figure 1, presenting the results of the experiments conducted in ambient air at R = 0.1 and with a test frequency of 35 Hz. At a given ΔK, the 2050 T851 alloy exhibits slightly higher growth rates than the 2022 T851 and 8090 T651 alloys, the two latter ones presenting a very similar behaviour. A growth rate plateau is observed respectively at 3.10^{-9} m/cycle and 4.10^{-9} m/cycle for the 2050 T851 and 8090 T651 alloys, while it is not detected on the 2022 T851 alloy. The threshold value (ΔK_{th}) for the 2050 T851 alloy was evaluated at 3.5 MPa.$m^{1/2}$, which value is lower than those of the other alloys, respectively 4.2 MPa.$m^{1/2}$ and 4.3 MPa.$m^{1/2}$ for the 2022 T851 and 8090 T651 alloys.

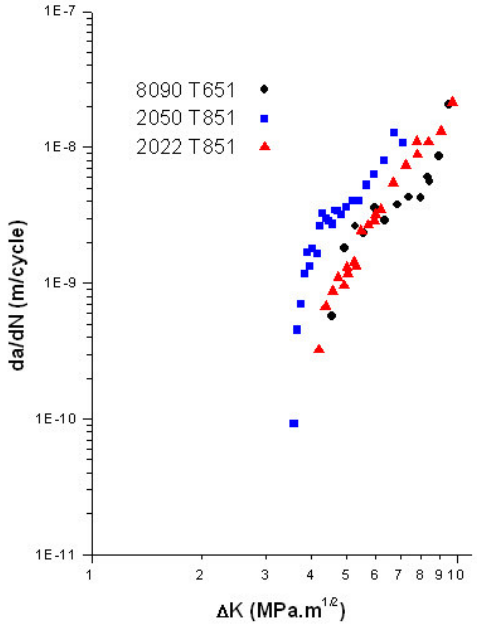

Figure 1 : da/dN vs. ΔK curves for the three studied alloys (R = 0.1, ambient air, 35Hz)

4.1 Crack closure contribution

Figure 2a presents the da/dN vs. ΔK_{eff} effective curves obtained for the three alloys in ambient air after closure correction. In the associated Figure 2b is plotted the evolution of the ration (1-U) vs. ΔK, with $U = \Delta K_{eff}/\Delta K$ as introduced by Elber [7]. In this diagram, it can be seen that the crack closure contribution, as represented by the evolution of (1-U) increases as the ΔK decreases. A more enhanced closure effect is shown on the 8090 T651 alloy as compared to the 2050 T851 and 2022 T851 alloys at a given ΔK amplitude. In the threshold domain, the 2022 T851 alloy exhibits the best effective resistance against crack propagation with lower crack growth rates for $\Delta K_{eff} < 2$ MPa.$m^{1/2}$.

The effective threshold ($\Delta K_{eff,th}$) for the 8090 T651, 2022 T851 and 2050 T851 alloys is respectively evaluated at 1.1 MPa.m$^{1/2}$, 1.4 MPa.m$^{1/2}$ and 0.5 MPa.m$^{1/2}$. Since the detrimental effect of atmospheric environment for most of the metallic materials fatigued at room temperature is known to be more accentuated in the near-threshold area [8, 9], these results suggest a much higher sensitivity of the 2050 T851 alloy to the ambient environment. To get a more in depth analysis of such a role of environment, reference tests were conducted in high vacuum.

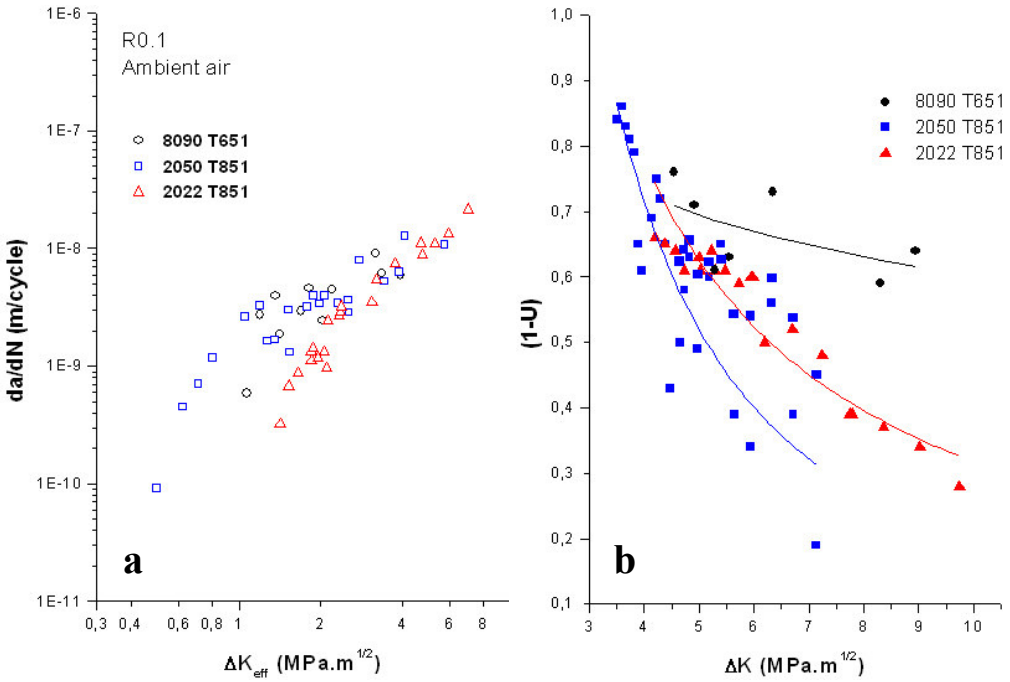

Figure 2 : (a) da/dN vs. ΔK_{eff} curves and (b) associated (1-U) =$\Delta K_{eff}/\Delta K$ curves for the three studied alloys (R0.1, ambient air, 35Hz)

4.2 Influence of the environment

Threshold tests in vacuum (P=7.8.10^{-6} Pa) were carried out on the 2050 T851 alloy, at R = 0.1. The Figure 3a and the Figure 3b present respectively the da/dN vs. ΔK and da/dN vs. ΔK_{eff} curves obtained for tests run in ambient air and in vacuum.

The Figure 3a shows that there is no significant difference, if not, in the behaviour of the 2022 T851 alloy in ambient air and in vacuum. But for the 2050 T851 and the 8090 T651 alloys, the resistance against crack propagation is substantially reduced in ambient air as compared to vacuum. The nominal threshold of the 2050 T851 and 8090 T651 alloys in vacuum is increased of about 26% (4.4 MPa.m$^{1/2}$) and 16% (5 MPa.m$^{1/2}$) respectively.

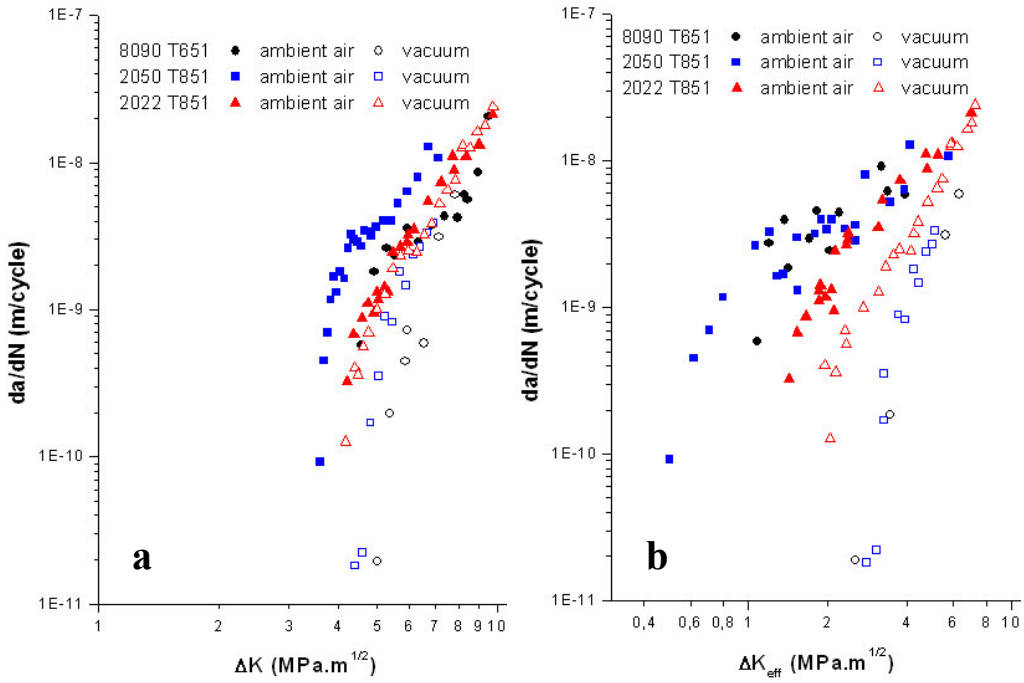

Figure 3 : (a) da/dN vs. ΔK and (b) da/dN vs. ΔKeff curves for the three studied alloys (R0.1, ambient air 35Hz, vacuum 30 Hz)

The intrinsic behavior (in vacuum and after closure correction) and the effective behaviour in air (after closure correction) are presented in Figure 3b. The 2050 T851 and 8090 T651 alloys present the same intrinsic behaviour and exhibit the best performance compared to the 2022 T851 alloy, especially in the near-threshold regime. Conversely, it can be noticed that in ambient air, the effective behaviour of the 2022 T851 alloy is better than that of the two other alloys. This phenomenon was previously observed on a 7075 alloy in T651 and T7351 conditions, tested in air and in vacuum [10]. The shearable precipitates contained in the 7075 T651 alloy were shown to promote a localization of plastic deformation, which leads in vacuum to a retarded crystallographic propagation (stage I-like regime [12]), whereas in ambient air the single slip mechanism is assumed to offer a preferential path for hydrogen embrittlement, which leads to a strongly accelerated propagation. The 7075 T7351 alloy contains larger less coherent precipitates which favour a wavy slip mechanism, leading in vacuum to a conventional stage II propagation [12] involving several slip systems, on which the ambient air has a little influence. These results are partially in accordance with those presented in [10]. The 8090 T651 alloy contains a shearable precipitation (δ') like the coherent η' phase in the 7075 T651 alloy, and the 2022 T851 alloy contains a less coherent precipitation (θ') like the 7075 T7351 alloy (with less coherent η' precipitation than at T651 temper). For the 2050 T851 alloy, the shearing of strong precipitates like T_1 [11] cannot be invoked to explain a behaviour similar to that of the 8090T651 alloy. SEM examinations were performed to get more precise information on the involved crack growth mechanisms.

4.3 Micro-fractographic SEM observations

The 2050 T851 alloy fracture surface of the specimen tested in ambient air shows a crack path presenting herringbone patterns (Figure 4a), with no significant change on the entire explored ΔK range. For 5 MPa.m$^{1/2}$ < ΔK < 7 Mpa.m$^{1/2}$, the fracture surface of the specimen tested in vacuum presents a fine ductile propagation (Figure 4b), assimilated to stage II regime. At ΔK = 5 MPa.m$^{1/2}$, a transition to a crystallographic propagation (stage I-like regime) is observed (Figure 5a), resulting in an important growth rate lowering. Crystallographic facets cover almost the whole fracture surface from ΔK = 5 MPa.m$^{1/2}$ down to ΔK_{th} (Figure 5b).

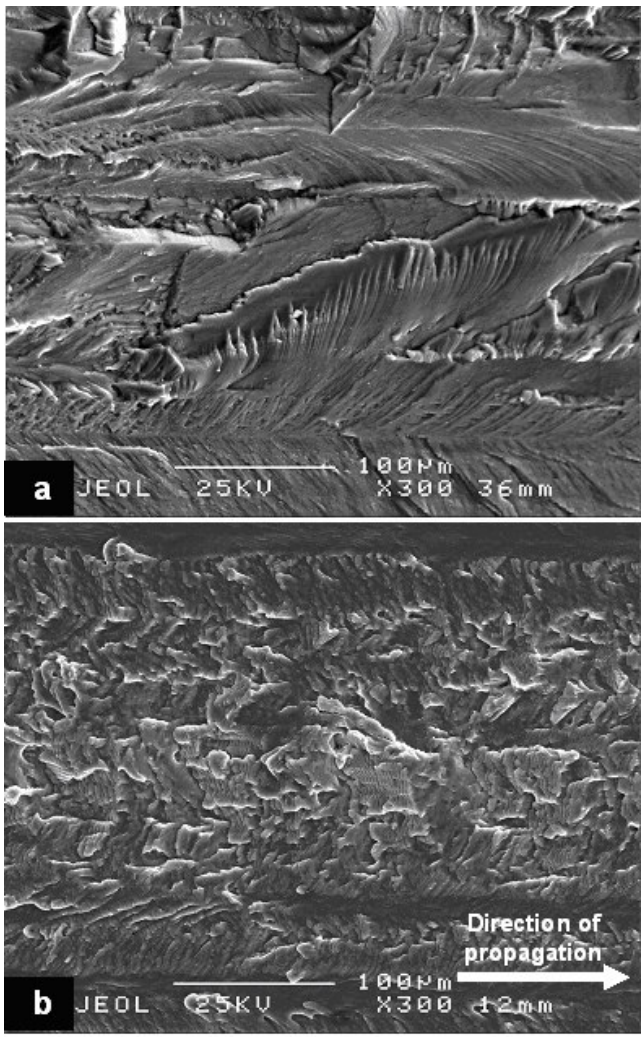

Figure 4 : SEM micrographs of the 2050 alloy at ΔK = 6 MPa.m$^{1/2}$ a) in air and b) in vacuum

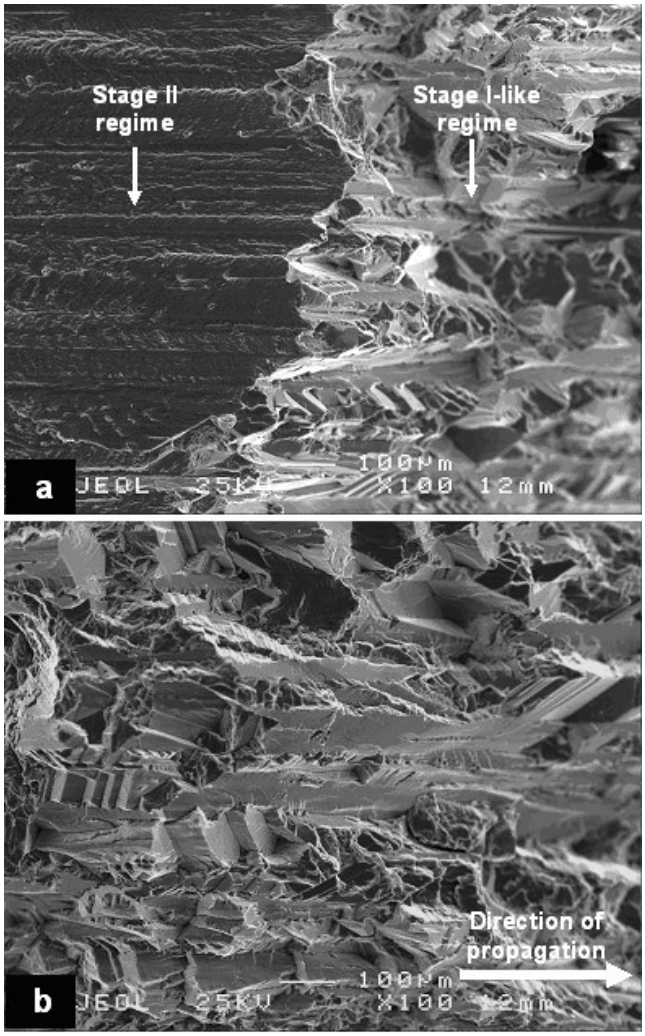

Figure 5 : a) transition from stage II regime to crystallographic stage I-like regime on the 2050 T851 alloy at $\Delta K = 5$ MPa.m$^{1/2}$ and b) crystallographic facets covering the fracture surface at $\Delta K = 4.5$ MPa.m$^{1/2}$

5 DISCUSSION

The detrimental effect of the ambient air on the resistance against crack propagation of the three studied alloys is demonstrated since the growth rates at a given ΔK are lower in vacuum than in ambient air (Figure 3a) and that the threshold values are higher in vacuum than in ambient air. The growth rate plateau observed in ambient air on both 2050 T851 and 8090 T651 alloys, as shown in Figure 1 and Figure 2a, is no more visible in vacuum (Figure 3a and Figure 3b), which indicates these plateaux result from an environmental effect, in accordance with previous observations [12].

Fracture surfaces observed on the 2022 T851 alloy are very similar to those on the 7075 T7351 alloy [4, 13], and show a stage II propagation regime in ambient air and in vacuum. The crack propagation mechanism is found to be a similar stage II regime for 8090 T651 and 2050 T851 alloys in ambient air, but in vacuum the crack propagation mechanism is shown to correspond to the stage I-like regime on the entire explored ΔK range for the 8090 T651 alloy [2, 3], whereas this regime appears only for $\Delta K \leq 5$ MPa.m$^{1/2}$ on the 2050 T851 alloy. These observations confirm that the T_1 precipitates in the 2050 T851 alloy do not particularly favour a localization of the deformation at the scale of each individual grain, which is generally required for the occurrence of a crystallographic propagation regime. The predominant mode is the stage II regime in this alloy (observed for $\Delta K > 5$ MPa.m$^{1/2}$).

For both environments (Figure 2a in air and Figure 3b in vacuum), the crack growth rates in 8090 T651 and 2050 T851 alloys are similar with respect to ΔK_{eff}, whereas the 8090 T651 exhibits a better resistance considering its nominal behavior (Figure 1 in air and Figure 3a in vacuum). The best performance of the 8090 T851 alloy results from a higher crack closure contribution.

6 CONCLUSION

The 2050 T851 alloy presents a higher environment sensitivity than the 2022 T851 and 8090 T651 alloys.

The predominant crack propagation mechanism in ambient air is the stage II regime for the three alloys.
In vacuum and in the near threshold area, the 2050 T851 alloy presents the stage I-like propagation regime, but the stage II regime is the predominant propagation mode for $\Delta K > 5$ MPa.m$^{1/2}$. However, the induced growth rates are similar to those obtained with the 8090 T651 alloy, presenting a stage I-like regime on all the explored ΔK range.

The resistance against crack propagation of the 2050 T851 alloy is comparable but slightly lower than that of the 2022 T851 and 8090 T651 alloys, the better performance of these two alloys being related to higher crack closure contributions.

REFERENCES

[1] S. Richard, C. Sarrazin-Baudoux, J. Petit, Fatigue crack propagation in new generation aluminium-lithium alloys, TMS 2009 Proceedings, to be published.

[2] R. Tintillier, Résistance à la propagation aux faibles vitesses des fissures de fatigue dans un alliage aluminium-lithium 8090, PhD Thesis, Université de Poitiers, 1988.

[3] N. Ranganathan, S.Q. Li, J.P. Bailon, J. Petit, On micromechanisms of fatigue crack growth in the 8090 T651 aluminum-lithium alloy, Materials Science and Engineering, A187 (1994) 37-42.

[4] C. Gasquères, Fissuration par fatigue et ténacité d'alliages d'aluminium 2xxx à 223K, Phd Thesis, Université de Poitiers, 2006.

[5] J.C. Newman, W. Elber, Mechanics of Fatigue Crack Closure, American Society for Testing Materials Pub., Philadelphia, 1988.

[6] M. Kikukawa, M. Jono, S. Mikami, Fatigue crack propagation and crack closure behavior under stationary varying loading-tests results of aluminium alloy, Journal of the Society on Materials Science, 31 (1982), 438-487.

[7] W. Elber, The significance of crack closure, in: Damage Tolerance in Aircraft Structures, American Society for Testing Materials, Philadelphia, 1970, pp. 230-242.

[8] J. Petit, G. Hénaff, C. Sarrazin-Baudoux, Mechanisms and modelling of near-threshold fatigue crack propagation, in: J.C. Newman, R.S. Piascik (Eds.), Fatigue Crack Growth Threshold, Endurance Limits and Design, American Society for Testing Materials, Philadelphia, 2000, pp. 3-30.

[9] R.P. Wei, Some aspects of environment-enhanced fatigue crack growth, Engineering Fracture Mechanics 1 (1968) 633-651.

[10] J. Petit, J. de Fouquet, G. Hénaff, Influence of ambient atmosphere on fatigue crack growth behaviour of metals, in: A. Carpinteri (Ed.), Handbook of Fatigue Crack vol. 2, Elsevier Science B.V., Amsterdam, 1994, pp. 1159-1203.

[11] C.P. Blankenship, E. Hornbogen, E.A. Starke, Predicting slip behavior in alloys containing shearable and strong particles, Materials Science and Engineering 169 (1-2) (1993) 33-41.

[12] J. Petit, G. Hénaff, C. Sarrazin-Baudoux, Environmentally-assisted fatigue in a gaseous atmosphere, in : J. Petit, P. Scott (Eds.), Comprehensive Structural Integrity, Elsevier, Oxford, 2003, pp. 211-280.

[13] P. Renaud, Influence de la structure sur le comportement en fatigue d'un alliage d'aluminium 7075 (AZ5 GU), PhD Thesis, Université de Poitiers, 1982.